A NEW COMPUTATIONAL TECHNIQUE FOR RE-ENTRY FLOW CALCULATIONS BASED UPON A SHOCK-FITTING TECHNIQUE FOR UNSTRUCTURED GRIDS

M. Onofri[1], **R. Paciorri**[1], **R. Pepe**[2], **A. Bonfiglioli**[2], **A. D'Angola**[2], **and G. Colonna**[3]

[1]*Centro Ricerche Aerospaziali Sapienza, Via Eudossiana 18, 00183 Roma Italy*
[2]*Università della Basilicata Scuola di Ingegneria, V.le dell'Ateneo Lucano n. 10, 85100 Potenza Italy*
[3]*IMIP, CNR Via Amendola 122/D - 70126, Bari, Italy*

Abstract

An in-house developed, 2D/3D unstructured CFD solver has been extended to deal with a mixture of thermally perfect gases in chemical non-equilibrium. The Euler equations have been coupled with a state-to-state kinetic model for argon plasma. The spatial discretization uses compact stencil Residual Distribution Schemes and shock waves can be modelled using either shock-capturing or shock-fitting. Promising results have been obtained using the shock-fitting approach for a 2D hypersonic flow past the fore-body of a circular cylinder.

1. INTRODUCTION

Modern CFD tools used in the aero-thermodynamic design and analysis of space re-entry vehicles rely upon the use of unstructured meshes: NASA's FUN3D and DLR's TAU codes are two such examples. On the one hand, unstructured-grid codes offer greater flexibility than structured-grid ones in tackling complex geometries and allow to automatically adapt the mesh to the local flow features. On the other hand, the strong shocks that characterise the hypersonic regime challenge the capability of unstructured codes to deliver accurate results much more than it happens to be the case with their structured-grid counterpart. Stagnation point anomalies [Gno07] are the most notable trouble into which state-of-the-art unstructured grid codes incur. These deficiencies have led to either look for better (e.g. mesh-independent) discretization schemes [Gno06, SK13] or to the use of locally prismatic grids (which mimic structured grids) around the shocks [CBD$^+$07]. The latter approach complicates the mesh generation task and is unlikely to be applicable wherever complex shock interactions occur; the quest for better discretization schemes seems to be hindered by intrinsic limitations in the shock-capturing approach, in particular the existence of an inner shock structure that is a purely numerical artefact. The aforementioned limitations manifest themselves through the reduction of the order of accuracy that is observed [CC99] within the entire shock-downstream region when shock-capturing codes are used.

We believe that it may pay off to undertake a more radical approach and revive the shock-fitting ideas within the unstructured-grid framework.

Shock-fitting discretizations based on the so-called "boundary" variant of the technique have been in use until the mid 90s [MWP94, Men95] to simulate supersonic and hypersonic flows: only the strong bow shock was fitted and made to coincide with the upstream boundary of a structured mesh; all other shocks were captured. The "floating" variant of the shock-fitting technique, although more versatile since it allows to fit also the embedded shocks, is algorithmically complex, so that only a few three-dimensional calculations have been reported in the literature [YK82]. Recent applications of the "boundary" shock-fitting technique in conjunction with high-order schemes on structured meshes have been reported in [PPWZ11], where it is used to perform DNS of compressible turbulence in chemical and thermal non-equilibrium conditions.

In recent years, some of the authors have developed an unstructured, shock-fitting algorithm that has been applied to the simulation of steady inviscid flows of a perfect gas in both two [PB09] and three spatial dimensions [BGPS13]. This unstructured version of the shock-fitting technique combines features of both the "boundary" and "floating" variants that had been proposed in the structured grid setting: it therefore allows not only to fit the bow shock, but also the embedded shocks. Moreover, the geometrical flexibility offered by the use of unstructured triangular and tetrahedral meshes allows to deal much more properly with interacting shock [IBPS10, PB11] than it was possible in the structured-grid context.

In this paper we describe a joint effort with colleagues from an Italian world-class team working on plasma physics, aimed at including non-equilibrium effects in the unstructured shock-capturing and shock-fitting codes.

2. GOVERNING EQUATIONS

Given a control volume C_i, fixed in space and bounded by the control surface ∂C_i with inward[1] normal $\boldsymbol{n}$, the integral form of the governing conservation laws of mass, linear momentum and energy for an arbitrary mixture of thermally perfect gases in chemical non-equilibrium has the form:

$$\int_{C_i} \frac{\partial U}{\partial t}\,\mathrm{d}V = \oint_{\partial C_i} \mathbf{F}\cdot\boldsymbol{n}\,\mathrm{d}S + \int_{C_i} \mathbf{S}\,dV \tag{1}$$

where $\mathbf{F}$ is the inviscid flux vector and $\mathbf{S}$ the chemical source term:

$$\mathbf{F} = \begin{pmatrix} \rho_i \boldsymbol{u} \\ \rho \boldsymbol{u} H \\ \rho \boldsymbol{u}\boldsymbol{u} + p\, I_{d\times d} \end{pmatrix}, \quad \mathbf{S} = \begin{pmatrix} S_i \\ 0 \\ \mathbf{0} \end{pmatrix}. \tag{2}$$

In Eq. (2) $I_{d\times d}$ is the unit matrix of order d, where d is equal to 2 for two-dimensional (2D) flows and 3 for three-dimensional (3D) flows. The vector of conservative variables is $U = (\rho_i, \rho E, \rho \boldsymbol{u})^t$. The standard notation for the kinematic and thermodynamic variables is adopted: the symbol $\boldsymbol{u}$ denotes the flow velocity, ρ the total density, $\alpha_i = \rho_i/\rho$ is the concentration of the i^{th} species and ρ_i the corresponding density, p the static pressure, T the temperature, E and H the specific total internal energy and enthalpy, respectively. In this work a state-to-state approach is considered, then each internal energy level is convected as a single chemical species, so that a continuity equation must be used for each internal state that is accounted for in the chemical model [DCC03].

At high temperatures, the effects of the intermolecular forces on particles motion can be neglected, so that it is possible to consider a mixture of thermally perfect gases [And06], in which case the equation of state is given by Dalton's law:

$$p = \sum_{i=1}^{N_s} \rho_i R_i T = \rho R T \tag{3}$$

where T is the mixture temperature, R_i is the specific gas constant of the i^{th} chemical species, $R = \sum_{i=1}^{N_s} \alpha_i R_i$ the specific gas constant of the mixture and N_s the number of species. The total internal energy $E = e + \frac{\mathbf{u}\cdot\mathbf{u}}{2}$ is the sum of the kinetic energy and the mixture internal energy:

$$e = \sum_{i=1}^{N_s} \alpha_i\, e_i(T) \tag{4}$$

where $e_i(T)$ is the internal energy of the i^{th} chemical species.

For high temperature flows it is not possible to neglect the electronic, vibrational and rotational energy excitation, so that it is not possible to assume that the gas is calorically perfect. Internal energy is given by the sum of a translational contribution e_i^t, a contribution due to excitation of the internal energy modes e_i^i and the formation enthalpy h_i^f [VK65]:

$$e_i = e_i^t + e_i^i + h_i^f. \tag{5}$$

Since the translational energy is assumed to be completely excited, the translational energy reads:

$$e_i^t(T) = \frac{3}{2} R_i T \tag{6}$$

[1]The use of inward normals is a convention in use since the early developments of this class of schemes.

while the internal energy can be sub-divided into three contributions: rotational (r), electronic (s) and vibrational (v):

$$e_i^i = e_i^r + e_i^e + e_i^v. \tag{7}$$

Concerning the atomic species, the rotational and vibrational energy is zero, so that the internal energy is only due to the electronic energy. Expressions for internal energy contributions are given by statistical mechanics [LL80], [CCD12].

In a state-to-state model, the internal energy of the monoatomic species is only given by the sum of the translational energy e_i^t and formation enthalpy h_i^f, since the excited electronic levels are convected as single chemical species [DCC03, KC11]:

$$e_i(T) = \frac{3}{2} R_i T + h_i^f \tag{8}$$

The Atomic distribution function (ADF) can be obtained in each point in space, considering the molar densities of each electronic excited species.

Chemical source terms S_i in Eq. (1) are given by the law of mass action [VK65]:

$$S_i = M_i \sum_{r=1}^{N_r} \left(\nu_{ir}^{''} - \nu_{ir}^{'}\right) \dot{\xi}_r \tag{9}$$

where:

$$\dot{\xi}_r = k_{fr} \prod_{s=1}^{N_s} \left(\frac{\rho_s}{M_s}\right)^{\nu_{sr}^{'}} - k_{br} \prod_{s=1}^{N_s} \left(\frac{\rho_s}{M_s}\right)^{\nu_{sr}^{''}} \tag{10}$$

In Eq. (10) k_{fr} and k_{br} are the forward and backward reaction rates and $\nu_{ir}^{'}$ and $\nu_{ir}^{''}$ are the stoichiometric coefficients for the products and reagents. Reaction rates depend upon the chosen collisional model [CCD12].

3. REDUCED STATE-TO-STATE MODEL FOR AN ARGON PLASMA

In this work we have considered a quasi-neutral argon plasma, i.e. the molar density of the positive particles is assumed to be equal to the molar density of the negative particles.

A precise description of an argon plasma in non-equilibrium would require a collisional-radiative model. This implies that not only the chemical reactions between the various species should be accounted for, but also all possible transitions between atomic electronic excited levels [Vlc89]. Furthermore, the energy distribution of the free electrons may follow a non-Maxwellian distribution function. Due to the extremely high computational cost, this type of modelling cannot be used in the context of a multidimensional CFD approach.

For an argon plasma, a good compromise is to consider a reduced number of electronic excited levels for the atomic species. Another compromise is to use a Maxwellian electronic energy distribution function (EEDF) for the electrons, which amounts to define a single temperature for the electrons (T_e). Moreover, we have made the hypothesis of thermal equilibrium between the electrons and the heavy particles, which amounts to use a single temperature model with $T_e = T$. In our model we take into account only three chemical species: the neutral atoms Ar, the positive ions Ar^+ and the electrons e^-. Following [CC03], we consider a two-levels system for the neutral atom, with the ground state Ar^0 and the $4s$ metastable state Ar^*, while we consider only the ground state for the positive ion Ar^+. Chemical species are reported in table 1. We include metastable argon atoms since ionisation of the excited atoms is caused by collision with particles of lower energies, so that the role of excitation and ionisation from metastable state cannot be neglected.

Table 1. Chemical species considered in the model

Chemical Species	Symbol	Formation energy (eV)	Statistical weight
Ground	Ar^0	0.0	1
Metastable	Ar^*	11.55	6
Positive Ion	Ar^+	15.76	1
Electron	e^-	0.0	0

Table 2. Chemical processes considered in the model

Description	Electron-Atom (e-A)	Atom-Atom (A-A)
Ionization from Ar^0	$Ar^0 + e^- \rightleftharpoons Ar^+ + e^- + e^-$	$Ar^0 + Ar^0 \rightleftharpoons Ar^+ + e^- + Ar^0$
Excitation	$Ar^0 + e^- \rightleftharpoons Ar^* + e^-$	$Ar^0 + Ar^0 \rightleftharpoons Ar^* + Ar^0$
Ionization from Ar^*	$Ar^* + e^- \rightleftharpoons Ar^+ + e^- + e^-$	$Ar^* + Ar^0 \rightleftharpoons Ar^+ + e^- + Ar^0$

As shown in Tab. 2, the chemical processes we account for are: electron-atom and atom-atom ionization (recombination) and electronic excitation (de-excitation). Photoionisation and photo-recombination are not included in the model, since their contribution is negligible compared to electronic and atomic processes [ZR67].

Both the forward and backward rate coefficients of the electron-atom processes have been computed for different values of the electron temperature, integrating the cross section over the corresponding Maxwellian EEDF. These rate coefficients have been fitted to reduce the computational cost.

The forward rate coefficients for the atom-atom processes have been taken from [BG78, Vlc89]:

$$k_{fr} = b_p \sqrt{T} (\varepsilon_{pq} + 2kT) e^{-\varepsilon_{pq}/k_B T}. \tag{11}$$

where k_B is the Boltzmann constant, ε_{pq} is the difference between the formation energies of the chemical species involved in the reaction and b_p is a coefficient depending on the chemical process.

Concerning the atom impact processes, the backward rate coefficients have been obtained using the detailed balance principle:

$$k_{br} = \frac{k_{fr}}{K_{eq_r}} \tag{12}$$

The equilibrium constants K_{eq_r} that appear in Eq. (12) are easy to compute once the ionization equilibrium constant K^I_{eq} is known [CCD12]:

$$K^I_{eq} = \frac{[Ar^+][e^-]}{[Ar]} = \frac{[Ar^+][e^-]}{[Ar^0] + [Ar^*]} \tag{13}$$

In Eq. (13) the concentrations are those at equilibrium and the equilibrium constant K^I_{eq} has been directly computed from the complete partition functions of Ar and Ar^+ and then fitted as a function of the temperature T.

4. NUMERICAL METHOD

In the next two paragraphs the shock-capturing code and the shock-fitting algorithm that have been used in this study will be briefly described. The shock-capturing discretization will be presented first, since it is also used in the shock-fitting approach to solve the governing PDEs in the smooth regions of the flow-field.

4.1. Shock-capturing

The `eulfs` code is an in-house, unstructured CFD solver that has been developed over the last fifteen years; see [Bon00] for a detailed description of its basic features. It relies on Fluctuation Splitting (FS), or Residual Distribution [DPSR93, vdWDID99, Abg06] schemes for the spatial discretisation. In the FS approach the dependent variables are stored at the vertices of the computational mesh which is made up of triangles in the 2D space, and tetrahedra in 3D and are assumed to vary linearly and continuously in space. The inviscid flux balance Φ^e (also referred to as the cell residual or cell fluctuation) is evaluated over each triangular/tetrahedral element e by means of a conservative linearisation [DvdW99] based on the parameter vector: $Z = \sqrt{\rho}\,(\alpha_k, H, \boldsymbol{u})^T$, $k = 1, .., N_s$ and scattered to the element vertices using signals Φ^e_i, see Fig. 1(a). Within a cell e, the signals have to sum up to the net flux for conservation: $\sum_{i \in e} \Phi^e_i = \Phi^e$.

The nodal residual is then assembled by collecting fractions Φ^e_i of the net fluxes Φ^e associated with all the elements by which the node i is surrounded, as schematically shown in Fig. 1(b).

The various FS schemes proposed in the literature differ by the way cell residuals are split into signals. It is possible to construct schemes that depend linearly upon the solution (when solving a linear PDE) and are either monotonicity

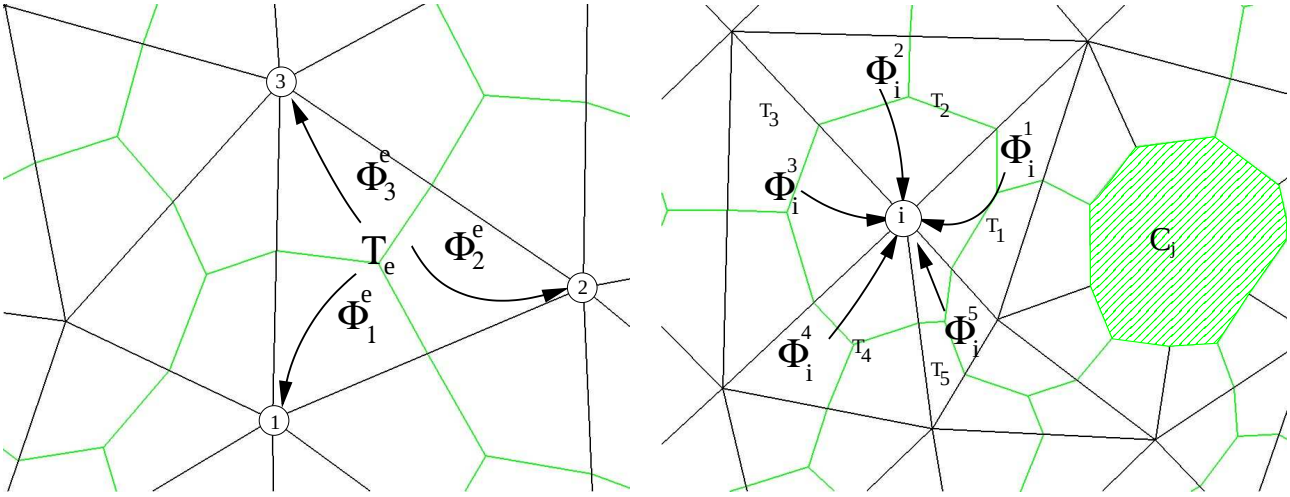

(a) The flux balance of triangle e is scattered among its vertices.

(b) Grid-point i gathers the fractions of cell residuals from the surrounding cells.

Figure 1. Residual distribution concept.

preserving, but limited to first order of accuracy, which is the case of the N scheme, or, if second order accurate, may lead to oscillatory behaviour in the neighbourhood of a captured discontinuity, which is the case of the LDA scheme. A non-linear scheme which captures the discontinuities monotonically and preserves second order of accuracy in smooth regions of the flow-field can be constructed by using a solution-dependent weighting function which blends the linear N and LDA schemes in such a way that the former scheme is activated only in the neighbourhood of the captured discontinuities whereas the latter is used elsewhere.

Using a fluid, such as the four species Argon described in Sect. 3, in which all species have the same number of degrees of freedom, the thermodynamic pressure is an homogeneous function of degree 2 in the components of the parameter vector; as shown in [DvdW99], this circumstance allows to generalise in a straightforward manner to chemical non-equilibrium flows the Roe-type conservative linearisation originally proposed in [DRS93] for a calorically perfect gas. With fluids made of different kind of species (e.g. mono and diatomic), or when also thermal non-equilibrium is accounted for, the conservative linearisation becomes more complex. This was the reason for choosing an argon plasma in the early development phase of the non-equilibrium CFD solver.

4.2. Shock-fitting

The unstructured shock-fitting algorithm consists of two key ingredients: *i*) a local re-meshing technique that constructs a time-dependent mesh in which the fitted discontinuities are internal boundaries of zero thickness and *ii*) an algorithm for solving the Rankine-Hugoniot jump relations that provides the Lagrangian velocity of the discontinuity and an updated set of dependent variables within the downstream side of the fitted shock. More precisely, in two space dimensions the fitted shock fronts are made of polygonal curves, i.e. a connected series of line segments (which we call the shock edges) that join the shock points. Two sets of flow states, corresponding to the upstream and downstream sides of the discontinuity, are assigned to each of the shock-points located on either side of the shock front. The downstream state and the shock speed are computed according to the Rankine-Hugoniot jump relations and the fitted shock is allowed to move throughout a background triangular mesh that covers the entire computational domain. At each time step, a local, constrained Delaunay triangulation is applied in the neighbourhood of the shock front to ensure that the edges that make up the shock front are also part of the triangular grid that covers the entire computational domain. This is what we refer to as the “shock-fitting” grid, which differs from the background one only in the neighbourhood of the shock front. The fitted shocks are treated as interior boundaries by the same shock-capturing code described in Sect. 4.1 which is used to solve the discretised governing equations in the smooth regions of the flow-field.

Only minor changes are required in the shock-fitting algorithm to account for real gas effects. In particular, modeling the bow shock as a partly dispersed shock wave [VK65], the concentration of the chemical species passes un-changed through the bow shock.

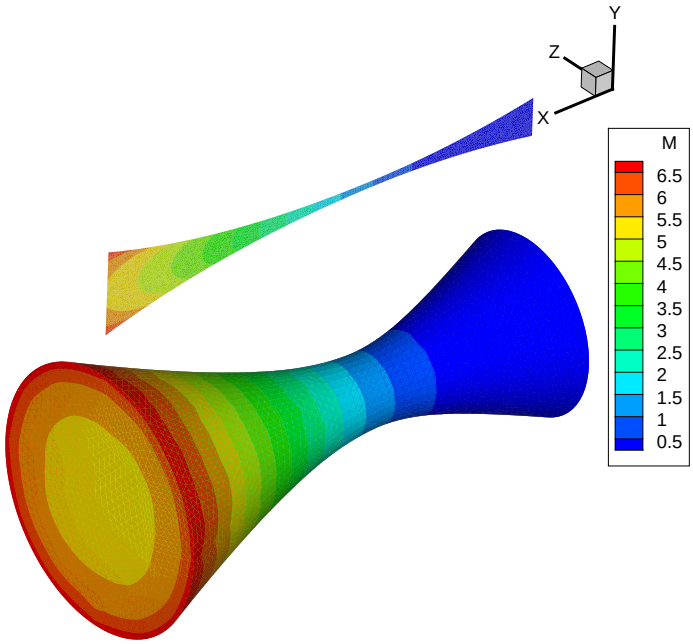

Figure 2. Flow in a converging-diverging nozzle: 2D and 3D geometries flooded by Mach number

5. NUMERICAL RESULTS

5.1. Flow in a converging-diverging nozzle

In order to validate the chemical model implemented within the `eulfs` code, results obtained from the 2D and 3D simulation of the flow through a converging-diverging nozzle have been compared with those obtained using a Q1D code developed at IMIP-CNR [CC01, CTG01]. In this reference code, the inviscid Q1D conservation equations are solved using a space-marching algorithm and are coupled with state-to-state kinetics and Boltzmann equation for free electron transport and the rates of electron collision processes are obtained by integrating the electron impact cross section over the EEDF. Therefore, in order to make the code-to-code validation meaningful, it has been necessary to downgrade the chemical model available in the IMIP-CNR code to make it identical to the one, described in Sect. 3, that has been implemented within the `eulfs` CFD code. The analytical area distribution of the converging-diverging nozzle is given in Tab. 2(a) whereas Tab. 2(b) shows the reservoir test conditions. In the 2D/3D simulations the total temperature, total pressure and flow angles have been specified along the subsonic inlet section and the metastable argon concentration has been set equal to that obtained considering a Boltzmann distribution for the electronic levels. The flow is supersonic at the outflow section and thus requires no boundary condition there. Figure 2 shows the 2D and 3D geometries with Mach iso-contours superimposed: the 2D grid is made of 4439 grid-points and 8447 triangles and the 3D grid is made of 28581 grid-points and 155667 tetrahedral cells. The 2D/3D simulations use the second order accurate LDA scheme for the spatial discretization.

(a) Area distribution.

x	**area**
$-0.3 < x < 0.0$	$A(x) = 0.010 + 0.6x^2$
$0.0 < x < 0.5$	$A(x) = 0.010 + 0.39\,x^2 + 0.26\,x^3$

(b) Test conditions.

Physical quantity	
Total pressure	10^5 Pa
Total temperature	5000 K
Ionisation degree	10^{-7}

Table 3. Flow in a converging-diverging nozzle

Figure 3 shows a comparison of the area weighted distributions along the nozzle axis; data include: the molar fractions of

ions and metastable argon, static temperature and Mach number. The 2D and 3D results are superimposed, despite the fact that the 2D grid is somewhat finer than the 3D one. The comparison between the 2D/3D calculations and the reference Q1D calculation can also be considered satisfactory, given the different numerical models, inlet boundary conditions and grid resolutions being used and points to the correct implementation of the chemical model.

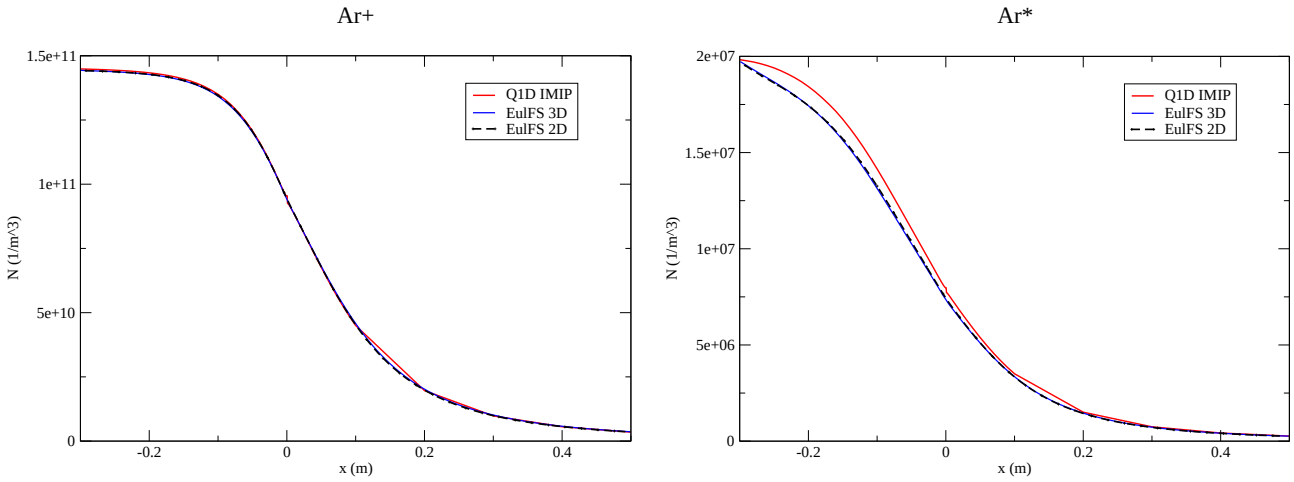

(a) Argon ions: Ar^{+}. (b) Metastable argon: Ar^{*}.

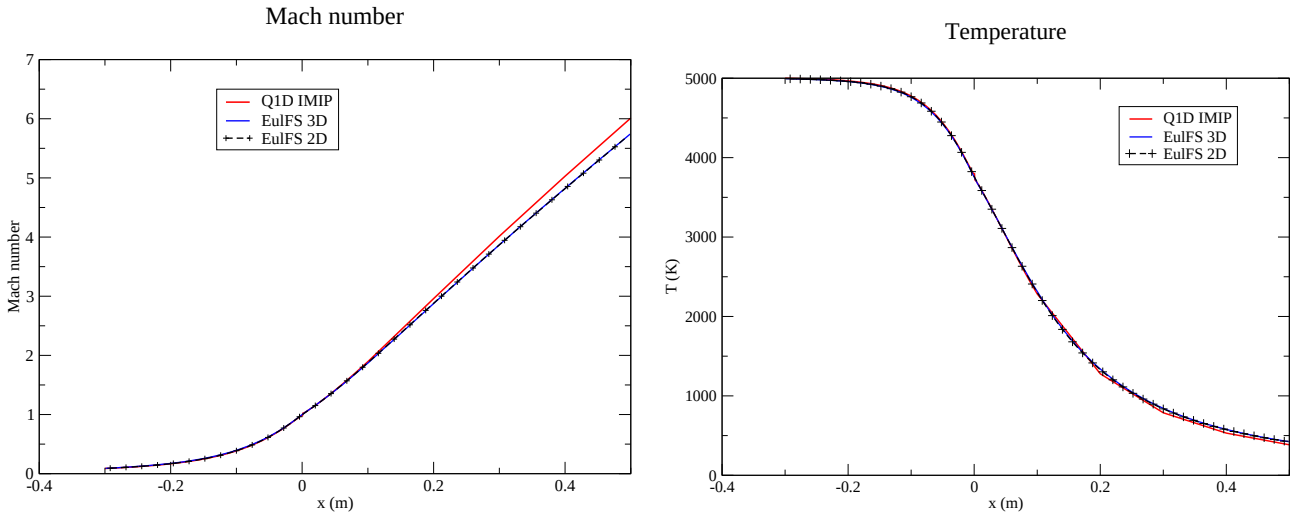

(c) Mach number. (d) Temperature.

Figure 3. Flow in a converging-diverging nozzle: distributions along the nozzle axis.

5.2. 2D hypersonic flow past the fore-body of a circular cylinder

Hypersonic flows over blunt bodies are characterised by strong non-equilibrium conditions. For an hypersonic flow in argon, ionisation and electronic excitation may significantly affect the macroscopic physical quantities, such as temperature or Mach number, within the entire flow field surrounding the body.

In this work we have considered the 2D hypersonic flow past the fore-body of a circular cylinder in order to conduct a comparative assessment of the predictive capabilities of the alternative shock-capturing and shock-fitting options available in the unstructured solver. The grid used for the shock-capturing calculation and also as the background triangulation in the shock-fitting calculation is made of 4723 nodes and 9097 elements; the shock-fitting grid at steady-state, which differs from the background triangulation only in the neighbourhood of the fitted shock, has 5029 gridpoints and 9348 triangles. In all calculations presented herein, the spatial discretization relies upon the first order accurate N scheme.

Free-stream conditions are given in Tab. 4: due to the low free-stream temperature, the shock-upstream flow is in equilibrium conditions and made only of neutral argon.

Table 4. Free-stream conditions

Physical quantity	Free-stream Value
M_∞	11
p_∞	543.95 Pa
T_∞	298.7 K
u_∞	3536.28 m/s

Figure 4 shows the static temperature (Fig. 4(a)) and Mach number (Fig. 4(b)) iso-contours computed by means of shock-capturing (lower half of the frames) and shock-fitting (upper half). It is clear from the comparison between the two

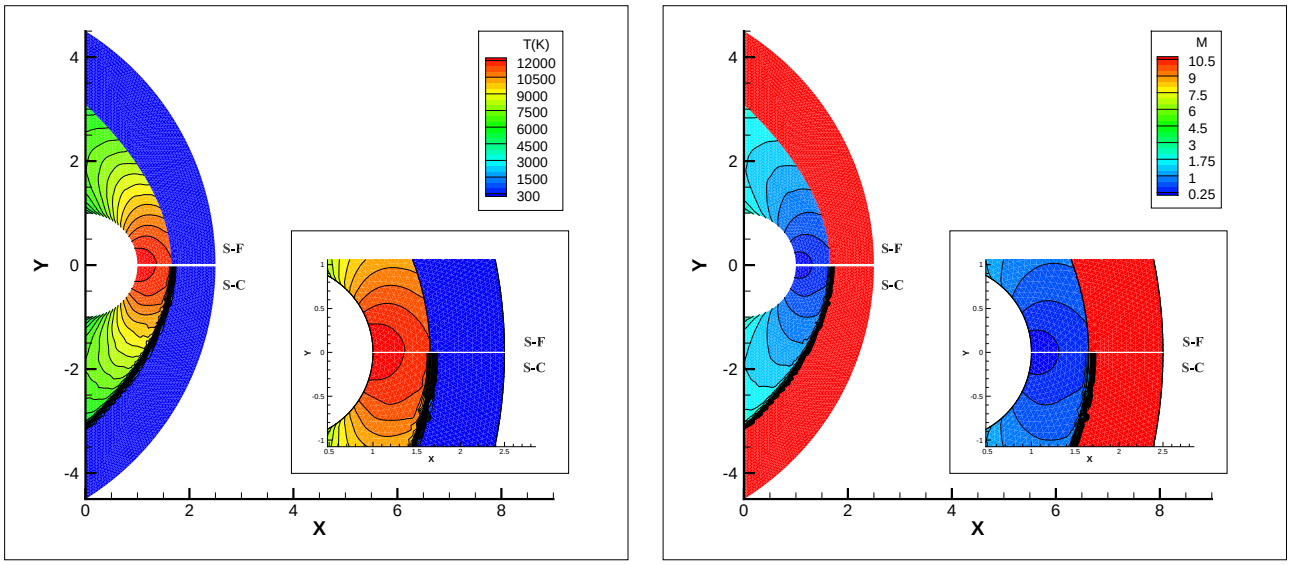

(a) Temperature (K) (b) Mach number

Figure 4. Comparison of shock capturing (S-C) and shock fitting (S-F) solutions.

sets of calculations that shock-fitting gives a much more realistic shock-thickness than does shock-capturing, without the need to adapt the mesh in the shock-normal direction, as would be the case if mesh adaptation was used in conjunction with the shock-capturing solver. The remarkable thickness of the captured bow-shock is particularly evident in Fig. 5(a), where symbols denote the intersections of the stagnation streamline (the x-axis) with the triangular grid. Even though the shock-capturing solution recovers the "exact" post-shock state, all those flow states that are inside the shock are a mere numerical artifact that also affect the chemistry, as we shall describe later. Moreover, the better description of the bow shock provided by shock-fitting has a clear, beneficial impact also on the smooth flow within the entire shock layer: both the temperature and Mach iso-contours within the shock-downstream region are smoother in the shock-fitting solution than they are in the shock-capturing one, see Fig. 4.

Finally, we observe that the chemical activity in the flow-field is the consequence of the temperature rise across the bow shock; this is evident from Fig. 5(b), which shows the molar concentrations of metastable argon and argon ions along the stagnation streamline, for both sets of calculations. It is interesting to observe how the different modeling practices, capturing versus fitting, have also an impact upon the non-equilibrium chemistry within the shock-downstream region. Indeed, since the captured shock is remarkably thick, in the shock-capturing calculation chemical reactions are activated already *inside* the shock, whereas they occur just *behind* the fitted shock in the shock-fitting solution. Due to the memory effect of the non-equilibrium chemical model, the "artificial" chemical concentrations that are created inside the captured shock are also felt downstream of the shock-wave, even beyond the spatial location, see Fig. 5(b), were both the shock-capturing and shock-fitting solutions have reached the same post-shock temperature. Therefore, the molar concentrations computed by means of shock-capturing and shock-fitting differ behind the shock and the differences will eventually vanish only further downstream.

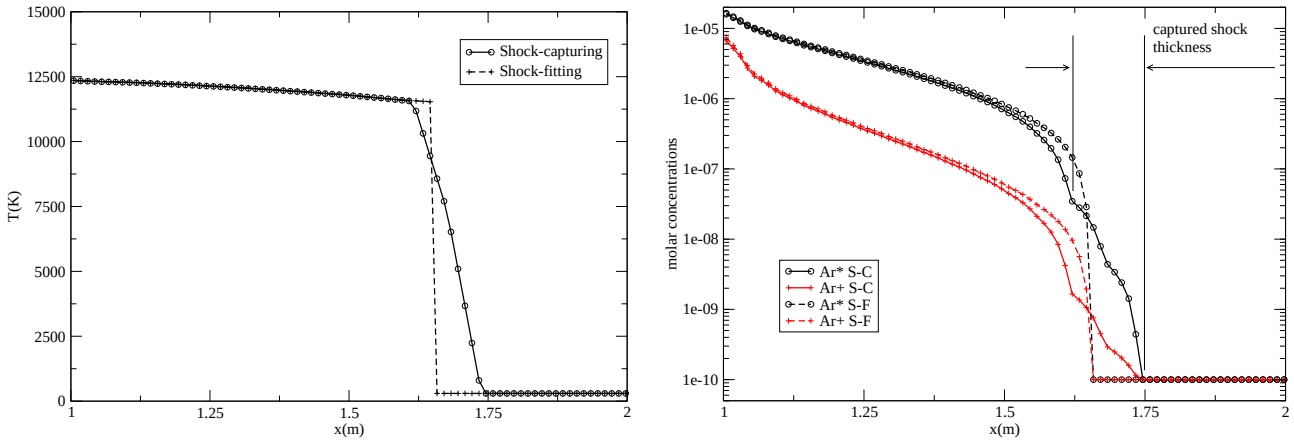

(a) Temperature

(b) Ar^* and Ar^+ molar concentrations

Figure 5. Comparison of shock-capturing (S-C) and shock-fitting (S-F) solutions along $y = 0$.

6. CONCLUSIONS

We have described the implementation of real gas, chemical non-equilibrium effects within an in-house developed, shock-capturing CFD code which uses compact-stencil, fluctuation splitting schemes on unstructured grids made of triangular and tetrahedral elements.

In presence of shock waves, the CFD code can either capture the shock or be coupled with a newly developed, unstructured, shock-fitting algorithm which treats the discontinuities as moving boundaries that border regions of the flowfield were a smooth solution to the governing PDEs exists. When operating in shock-fitting mode, the shock-capturing code is only used to solve the smooth regions of the flow field and it is left to the shock-fitting algorithm to enforce the Rankine-Hugoniot jump relations and preserve the species concentrations through the fitted shocks.

It has been numerically verified that fitting the shock waves provides a cleaner (compared to shock-capturing) description of the shock and shock layer that are encountered in typical hypersonic configurations.

Future developments include the inclusion of fluids other than the argon plasma examined here and of thermal non-equilibrium effects; these upgrades will in turn require the implementation of a more complex conservative linearization than the one used up to now.

REFERENCES

[Abg06] R. Abgrall. Residual distribution schemes: Current status and future trends. *Computers & Fluids*, 35(7):641 – 669, 2006. Special Issue Dedicated to Professor Stanley G. Rubin on the Occasion of his 65th Birthday.

[And06] J. D. Anderson. *Hypersonic and High-Temperature Gas Dynamics*. AIAA Education Series. AIAA, 2 edition, 2006.

[BG78] J. Bacri and A. M. Gomes. Influence of atom-atom collisions on thermal equilibrium in argon arc discharges at atmospheric pressure. *Journal of Physics D: Applied Physics*, 11(16):2185, 1978.

[BGPS13] A. Bonfiglioli, M. Grottadaurea, R. Paciorri, and F. Sabetta. An unstructured, three-dimensional, shock-fitting solver for hypersonic flows. *Computers & Fluids*, 73(0):162–174, 2013.

[Bon00] A. Bonfiglioli. Fluctuation splitting schemes for the compressible and incompressible euler and navier-stokes equations. *International Journal of Computational Fluid Dynamics*, 14(1):21–39, 2000.

[CBD+07] G. Candler, M. Barnhardt, T. Drayna, I. Nompelis, D. Peterson, and P. Subbareddy. Unstructured grid approaches for accurate aeroheating simulations. In *Fluid Dynamics and Co-located Conferences*. American Institute of Aeronautics and Astronautics, June 2007. AIAA 2007-3959.

[CC99] Mark H. Carpenter and Jay H. Casper. Accuracy of Shock Capturing in Two Spatial Dimensions. *AIAA Journal*, 37(9):1072–1079, September 1999.

[CC01] G. Colonna and M. Capitelli. Self-consistent model of chemical, vibrational, electron kinetics in nozzle expansion. *Journal of Thermophysics and Heat Transfer*, 15(3):308–316, July 2001.

[CC03] G. Colonna and M. Capitelli. The effects of electric and magnetic fields on high enthalpy plasma flows. In *Fluid Dynamics and Co-located Conferences*. American Institute of Aeronautics and Astronautics, June 2003. AIAA 2003-4036.

[CCD12] Mario Capitelli, Gianpiero Colonna, and Antonio D'Angola. *Fundamental Aspects of Plasma Chemical Physics*, volume XVII of *Springer Series on Atomic, Optical, and Plasma Physics*. Springer, 2012.

[CTG01] G. Colonna, M. Tuttafesta, and D. Giordano. Numerical methods to solve euler equations in one-dimensional steady nozzle flow. *Computer Physics Communications*, 138(3):213 – 221, 2001.

[DCC03] D. D'Ambrosio, G. Colonna, and M. Capitelli. Numerical prediction of non-equilibrium flows in hypersonic nozzles: State-to-state kinetics versus macroscopic models. In *Fluid Dynamics and Co-located Conferences*. American Institute of Aeronautics and Astronautics, June 2003. AIAA 2003-3549.

[DPSR93] H. Deconinck, H. Paillère, R. Struijs, and P.L. Roe. Multidimensional upwind schemes based on fluctuation-splitting for systems of conservation laws. *Computational Mechanics*, 11(5/6):323–340, 1993.

[DRS93] H. Deconinck, P.L. Roe, and R. Struijs. A Multi-dimensional Generalization of Roe's Flux Difference Splitter for the Euler Equations. *Computers and Fluids*, 22(2/3):215–222, 1993.

[DvdW99] G. Degrez and E. van der Weide. Upwind residual distribution schemes for chemical non-equilibrium flows. In *Fluid Dynamics and Co-located Conferences*. American Institute of Aeronautics and Astronautics, November 1999. AIAA 99-3366.

[Gno06] Peter Gnoffo. Semi-analytic reconstruction of flux in finite volume formulations. In *Aerospace Sciences Meetings*. American Institute of Aeronautics and Astronautics, January 2006. AIAA 2006-1090.

[Gno07] Peter Gnoffo. Simulation of stagnation region heating in hypersonic flow on tetrahedral grids (invited). In *Fluid Dynamics and Co-located Conferences*. American Institute of Aeronautics and Astronautics, June 2007. AIAA 2007-3960.

[IBPS10] M. S.. Ivanov, A. Bonfiglioli, R. Paciorri, and F. Sabetta. Computation of weak steady shock reflections by means of an unstructured shock-fitting solver. *Shock Waves*, 20(4):271–284, 2010.

[KC11] M.G. Kapper and J. L Cambier. Ionizing shocks in argon. part i: Collisional-radiative model and steady-state structure. *Journal of Applied Physics*, 109(11):113308–113308–14, 2011.

[LL80] L. D. Landau and E. M. Lifshitz. *Statistical Physics, Vol. 1*, volume 24. Oxford: Pergamon, 1980.

[Men95] S. Menne. Computation of non-winged vehicle aerodynamics in the low supersonic range. In J. J. Hunt, editor, *Aerothermodynamics for space vehicles*, volume 367 of *ESA Special Publication*, page 73, 1995.

[MWP94] S. Menne, C. Weiland, and M. Pfitzner. Computation of three-dimensional hypersonic flows in chemical nonequilibrium. *Journal of Aircraft*, 31(3):623–630, May 1994.

[PB09] Renato Paciorri and Aldo Bonfiglioli. A shock-fitting technique for 2d unstructured grids. *Computers & Fluids*, 38(3):715 – 726, 2009.

[PB11] R. Paciorri and A. Bonfiglioli. Shock interaction computations on unstructured, two-dimensional grids using a shock-fitting technique. *Journal of Computational Physics*, 230(8):3155 – 3177, 2011.

[PPWZ11] A. Prakash, N. Parsons, X. Wang, and X. Zhong. High-order shock-fitting methods for direct numerical simulation of hypersonic flow with chemical and thermal nonequilibrium. *Journal of Computational Physics*, 230(23):8474 – 8507, 2011.

[SK13] Eiji Shima and Keiichi Kitamura. Multidimensional numerical noise from captured shock wave and its cure. *AIAA Journal*, 51(4):992–998, February 2013.

[vdWDID99] E. van der Weide, H. Deconinck, E. Issman, and G. Degrez. A parallel, implicit, multi-dimensional upwind, residual distribution method for the Navier-Stokes equations on unstructured grids. *Computational Mechanics*, 23:199–208, 1999.

[VK65] W. G. Vincenti and C. H. Krüger. *Introduction to physical gas dynamics*, volume 26. Wiley, 1965.

[Vlc89] J. Vlcek. A collisional-radiative model applicable to argon discharges over a wide range of conditions. i. formulation and basic data. *Journal of Physics D: Applied Physics*, 22(5):623, 1989.

[YK82] Y. Yamamoto and K. Karashima. Floating shock fitting for three-dimensional inviscid supersonic flows. *AIAA Journal*, 20(1):9–17, January 1982.

[ZR67] Ya B Zel'dovich and Yu P Raizer. Physics of shock waves and high-temperature hydrodynamic phenomena. *New York: Academic Press, 1966/1967, edited by Hayes, WD; Probstein, Ronald F.*, 1, 1967.